Available online at www.sciencedirect.com
SCIENCE DIRECT®
Quaternary International 140–141 (2005) 103–120

Late Pleistocene–Holocene marsh episodes along the Carmel coast, Israel

R. Cohen-Seffer[a], N. Greenbaum[a,b,*], D. Sivan[c], T. Jull[d], E. Barmeir[e], S. Croitoru[e], M. Inbar[a]

[a]*Department of Geography and Environmental Studies, University of Haifa, Mt. Carmel, Haifa 31905, Israel*
[b]*Department of Natural Resources and Environmental Management, University of Haifa, Mt. Carmel, Haifa 31905, Israel*
[c]*Department of Maritime Civilizations and The Recanati Institute for Maritime Studies (RIMS), University of Haifa, Mt. Carmel, Haifa 31905, Israel*
[d]*NSF Arizona AMS Laboratory, Physics Building, University of Arizona, 1118 East Fourth St, Tucson, AZ 85721, USA*
[e]*Department of Radiology, Bnei Zion Medical Center, Haifa 31048, Israel*

Available online 18 July 2005

Abstract

Late Pleistocene–Holocene sequences in the southern Carmel coastal plain of Israel were obtained from two cores, 12 and 16 m deep, at the western and eastern longitudinal troughs, separated by a north–south "kurkar" sandstone ridge. The core sequences unconformably overlie the kurkar and were analyzed using X-ray radiography, grain size analysis, organic matter and water content. The sequences include (a) Brown sandy clay units, indicating terrestrial conditions of aeolian sand and dust deposition and pedogenesis dated between 20,200–19,650 and 9540–9130 cal. yr BP (western trough) and to 14,000–13,000 and 7680–7510 cal. yr BP (eastern trough). They are related to gradual warming and wetter climate when the coastline was far to the west; (b) overlying dark silty clay sediments, indicating fresh to brackish, shallow-water marsh with organic and fossil-rich, hydromorphic mineral soil, which prevailed at the western trough until 9010–8640 cal. yr BP (900 yr) and dried while the coastline was 1 km to the west. The marsh deposits were exposed for 3600 yr and populated by Pre-Pottery Neolithic and Chalcolithic settlements before they were covered by marine-aeolian sand at 5100 yr. The Kabara marshes at the eastern trough are asynchronous with the western marshes and prevailed from 7680 to 7510 cal. yr BP until the present. The genesis of these marshes may be related to the transition to a drier climate, resulting in an increasing frequency of large floods, as indicated by the high sedimentation rate, as well as to sea-level rise and its effect on groundwater level.

1. Introduction

Wetlands are widespread and exist in a large variety of hydrological conditions. Most contemporary worldwide coastal wetlands are Holocene in age and are generally related to sea-level rise. Stratigraphical sequences of wetlands serve as records for reconstructing paleoenvironments and identifying environmental changes (Orme, 1991; Mitsch and Gosselink, 1993).

The Late Pleistocene to Holocene sedimentary sequences in the coastal plain of Israel accumulated only in the troughs between longitudinal, north–south, Late-Pleistocene, calcareous aeolianite sandstone ridges, locally named 'kurkar' (Michelson, 1970). These sequences uncomformably overlie irregular topography of the kurkar. The Pleistocene sequence is composed of alternating kurkar sandstone, red loamy 'Hamra' paleosol, and sand, while in the troughs the younger units, mostly Holocene in age, include thick layers of dark-brown clays. Holocene marshy clay deposits, partly covered by sand, are found all along the Israeli coast and continental shelf. Sedimentological, palynological and faunal analyses show that these clay layers

*Corresponding author. Department of Geography and Environmental Studies, University of Haifa, Mt. Carmel, Haifa 31905, Israel. Tel.: +972 4 8240020; fax: +972 4 8249605.
E-mail address: noamgr@geo.haifa.ac.il (N. Greenbaum).

1040-6182/$ - see front matter © 2005 Elsevier Ltd and INQUA. All rights reserved.
doi:10.1016/j.quaint.2005.05.017

were deposited in freshwater to brackish marshes (Inbar and Sivan, 1984; Sneh and Klein, 1984; Galili and Weinstein-Evron, 1985; Sivan et al., 1999, 2004a; Kadosh et al., 2004). Gvirtzman and Wieder (2001) reconstructed a 53,000-yr paleoclimatic record based on a sequence of paleosols, aeolianites (kurkar) and dune sand along the coastal plain of Israel, using magnetic susceptibility, grain size distribution, clay mineralogy and soil micromorphology.

In spite of the numerous drillings (Fig. 1) at the eastern trough of Mt. Carmel coastal plain, the paleogeography of these marshes had not been studied. In the western trough of the Carmel coast, previous research suggested that the origin of the coastal marshes is related to sea-level rise, which was relatively rapid at the beginning of the Holocene (Sneh and Klein, 1984; Galili and Weinstein-Evron, 1985). Sivan et al. (2001, 2004b) reconstructed a Holocene sea-level curve and suggested that the quick drying-up of the coastal marshes at the beginning of the Holocene, while the sea level rose and the coastline was far to the west, is a result of climate fluctuations. Most coastal marshes along the Carmel coast dried up between 10,400 and 9550 cal. yr BP (Kadosh et al., 2004; Sivan et al., 2004a). The sands overlying this clay started to accumulate not earlier than 5100 yr BP (Kadosh et al., 2004).

The best paleoclimatic records in Israel are the stable isotope records from speleothems in caves on the western flanks of the mountainous area of Israel (Bar-Matthews et al., 1998, 1999; Frumkin et al., 1999, 2000) and from the eastern flanks (Vaks et al., 2003). Enzel et al. (2003) showed that rainstorms which affect north and central Israel control the flow regime into the Dead Sea and also affect the coastal area. Thus, the Dead Sea-level record may also serve as a comparative paleoclimatic indicator: rising lake level indicates relatively wetter climate and falling lake level represents drier conditions.

While Holocene sea-level changes are very well documented (Sivan et al., 2001) the climate records in this area are scarce. The closest climatological record to our study area is a short palynological record from Dor, about 2 km to the north (Fig. 1; Kadosh et al., 2004). We use our data from the cores, together with the various paleoclimatic records and sea-level curves (Lambeck and Bard, 2000; Sivan et al., 2004b) to reconstruct the paleoenvironment of the southern Mount Carmel coastal plain.

Human settlements were established over these dark clays shortly after the drying of the marshes (Galili and Weinstein-Evron, 1985). Prehistoric remains were dated to the Pre-Pottery Neolithic period (PPN), starting at about 10,300 BP (Bar-Yosef, 1998), up to the Chalcolithic period, about 7000–5100 BP (Garfinkel, 1999). Only during the Middle Bronze IIA, at about 4000 BP, did people start to settle on the kurkar hills along the coast (Broshi and Gophna, 1986; Raban, 1987; Gophna and Portugali, 1988).

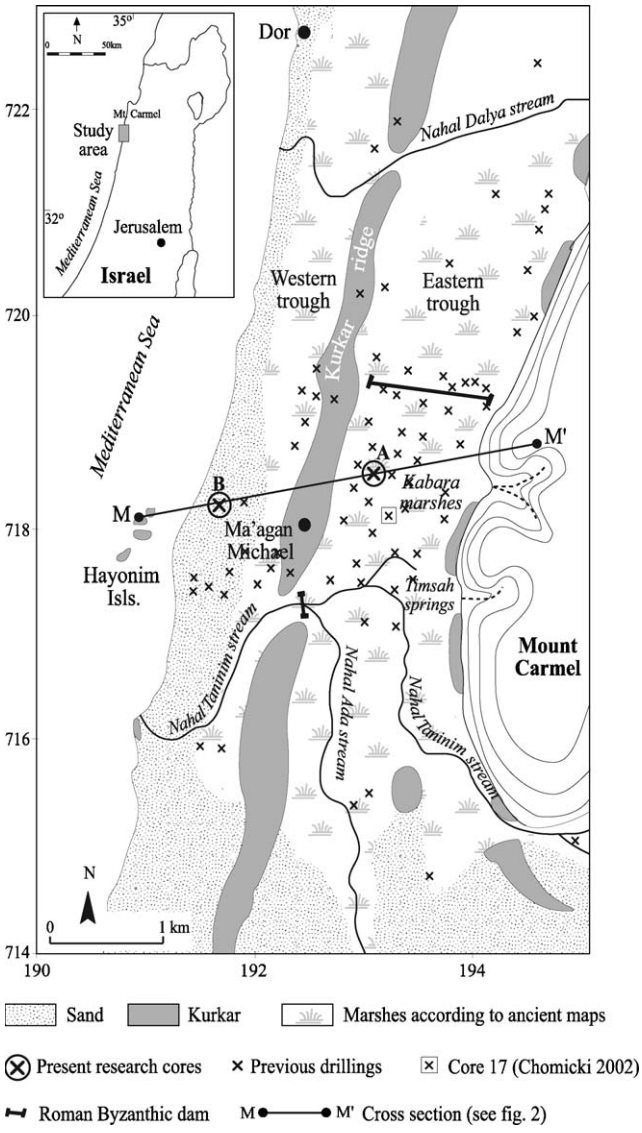

Fig. 1. Map of the southern Carmel coastal plain and the study area at the eastern (Kabara marsh) and western troughs. *Note*: The spatial distribution of the marsh is based on historical maps and reports (Schumacher, 1887; Mülinen, 1907; PEF, 1918; Caron, 1922). Note the large number of previous shallow drillings performed by the Geological Survey of Israel, the Israel Water Commission, Tahal Ltd., NRD Ltd., Michelson (1970).

2. Study area

The narrow (2–3 km wide) southern Carmel coastal plain of Israel is bounded by Mount Carmel on the east and the Mediterranean Sea on the west (Fig. 1). The study area is bordered in the west by a submerged kurkar ridge represented by the Hayonim Islands, while in the east the western flanks of Mt. Carmel form a vertical escarpment about 120 m above sea level. A continuous kurkar ridge

(up to 18 m above sea level) separates two elongated troughs, where marshes prevailed (Figs. 1 and 2). In the western trough, a thick sand unit covers the dark marsh clay sediments, while in the eastern trough clays are exposed on the surface. The marshes at the eastern trough are known as the 'Kabara marshes' (Fig. 1). To the north, the study area is bordered by the Nahal Dalia stream with a drainage area of 95 km^2. Nahal Taninim stream (100 km^2) and its main tributary Nahal Ada (100 km^2) cut through the southern part of the study area (Fig. 1). These streams usually flow from November to April, delivering water and sediments into the marshes during winter floods. The mean annual discharge of these streams was about $90 \times 10^6\,m^3\,yr^{-1}$ during the late 1950s and decreased to about $20 \times 10^6\,m^3\,yr^{-1}$ since the late 1980s due to intensive pumping of water (Israel Hydrological Service). From May to October all these streams are usually dry.

The permanent sources of water feeding the eastern wetlands are numerous fresh to saline springs, known as the Timsach Springs (Fig. 1), which are the northernmost outlet of the deeper Cenomanian carbonate aquifer (Guttman, 1998), and had a natural mean annual discharge of about $57 \times 10^6\,m^3\,yr^{-1}$ prior to 1960. These springs create, at present, a permanent inland brackish water body of about 0.1 km^2—a remnant of the past larger Kabara marshes (Almogi-Labin et al., 2002).

Previous research related the initiation of the Kabara marshes to the two Roman artificial dams that were constructed over Nahal Taninim near Ma'agan Michael and at the water divide between Nahal Taninim and Nahal Dalia (Fig. 1) in the 3rd century AD (Caron, 1922), as a part of the water supply system to ancient Caesarea (Porath, 2002). These dams created an artificial reservoir and increased the water level from approximately 0.8 to 2.8 m above the present sea level as determined by Chomicki (2002), based on 17 cores in the reservoir area, and paleontological, grain size, chemistry

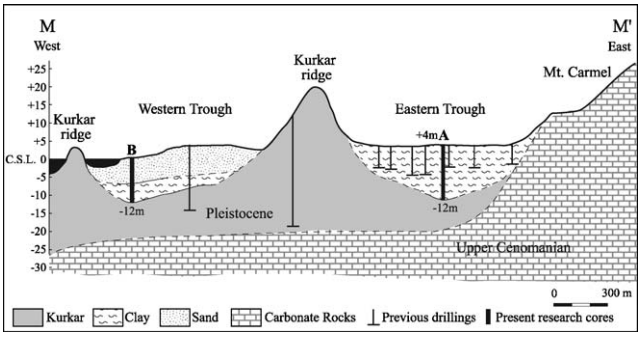

Fig. 2. A section across the study area reconstructed from previous and present study drillings and geological cross-sections (Michelson, 1970). *Note*: The Late Pleistocene–Holocene sediments in the troughs are unconformably deposited over the Pleistocene kurkar, which is unconformably deposited over Upper Cenomanian chalk and limestone. The location of the present drillings are at the deepest parts of the troughs.

and isotopic analyses. She indicated that the pre-reservoir wetland was a shallow marsh with brackish water. The construction of the dam improved water quality, but the area reverted to shallow brackish marsh when the dams were abandoned at the end of the Crusader period during the mid-13th century AD. Our research indicates that wetland conditions prevailed in the area thousands of years before the Roman dam was first built. Old maps (PEF, 1918) and historical evidence (Schumacher, 1887; Mülinen, 1907; Schiller, 1979) document the wide extent of the marshes during the last 200 yr (Fig. 1). This research aims at reconstructing the palaeogeography of the Carmel coast, based on a detailed analysis and dating the two cores at the western and eastern troughs.

3. Methods

The 3D stratigraphical reconstruction of the research area is based on about 70 drilling logs carried out for many purposes by different authorities (Fig. 1). These data enabled us to core at the deepest sites along a northeast–southwest cross-section (Figs. 1 and 2). Two cores were analyzed (Figs. 1, 2): Core A—in the eastern trough east of the kurkar ridge, where the topographical elevation is 4 m above sea level; and Core B—in the western trough west of the kurkar ridge, at the present coastline. Drilling reached the top of the underlying kurkar to 16 m depth for Core A and 12 m for Core B. The core diameter was 5 cm.

The clay sequences were X-rayed at the Department of Radiology of Bnei Zion Medical Center, Haifa, in overlapping segments of 12 cm each, at a scale of between 1:1 and 1:3. ENVI 3.2 picture-processing software was used for dividing the range of brightness into intervals and assigning a color to each interval (Campell, 1996). The ENVI processing was carried out in this research on the X-ray radiographs and on core photographs (Figs. 3 and 4).

Each core was cut in half longitudinally in the laboratory and described according to its sedimentological characteristics: color (after the Munsell color chart), stiffness and plasticity defined qualitatively by resistance to wire-cutting, fabric, and description of all coarse findings such as macro-fossils, kurkar clasts, and remains of organic matter. Structural description followed Collinson and Thompson (1989) and Potter et al. (1980).

The cores were systematically sampled every 10 cm and according to the findings, with 137 samples from Core A and 41 samples from Core B. The laboratory analyses included organic matter content, grain size distribution and water content. The sand fraction (2–0.063 mm) was separated using dry sieving, and the

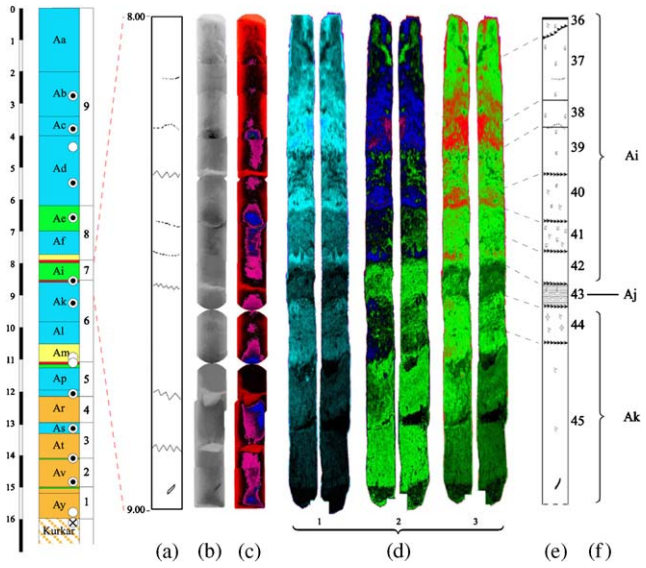

Fig. 3. Photograph processing of Core A between 8 and 9 m, using ENVI software which uses differential linear stretching and density slicing. The core-photograph processing allows the detection of sedimentary structures and stratigraphic contacts that cannot be seen visually or in X-ray radiography. (a) Schematic columnar section based on the core radiograph only. (b) Core radiograph. (c) Core-radiograph processing. (d) Stages in core-photograph processing. (e) Detailed stratigraphy of sub-units. (f) Generalized units. All the units are of the GB group. Possible scale differences between radiograph and photograph are smoothed in the stratigraphic sketch. Apparent contacts at 8.78 and 8.89 m are due to core breakage.

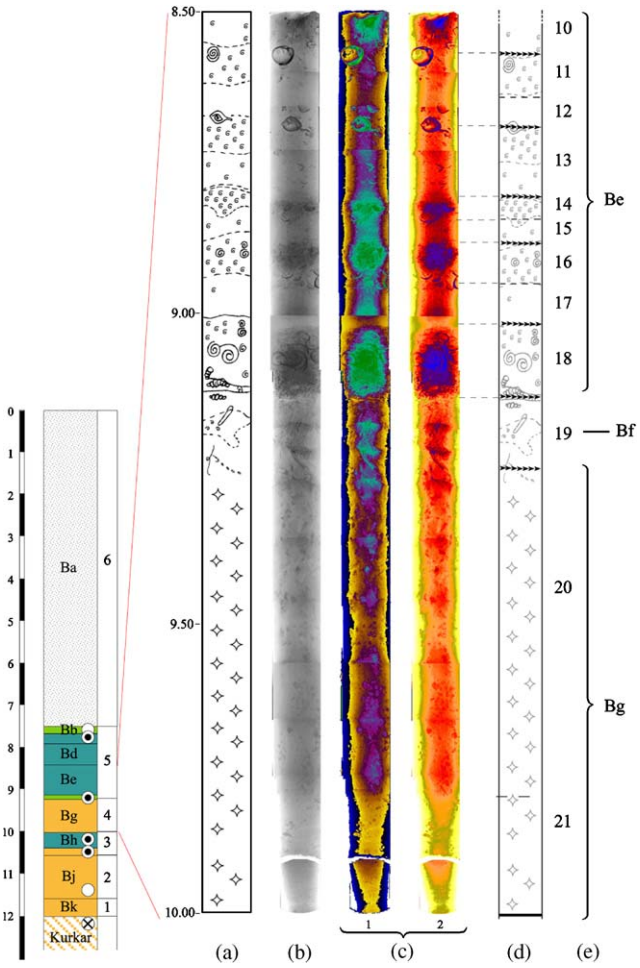

Fig. 4. Radiograph processing of Core B between 8.5 and 10 m using ENVI software which uses different linear stretching and density slicing. (a) Schematic column based on core radiograph only. (b) Core radiograph. (c) Stages in the radiograph processing. (d) Detailed stratigraphy of sub-units. (e) Generalized units. The radiograph processing emphasizes stratigraphic structures. Unit Bg is a structureless Br unit and the radiograph processing allows detection of possible internal variations. Unit Bf is a transitional unit. Unit Be is a GB unit with parallel bedding and changing concentration of macro-fossils.

silt and clay fractions (<0.063 mm) were analyzed using a Sedigraph 2000.

Twenty-two samples were ^{14}C-dated using the AMS technique: 14 at the NSF Arizona AMS Laboratory, Tucson, and 8 at the Institute of Particle Physics, Zurich, Switzerland (Table 1). The analyses were performed on the total organic carbon material extracted from the sediments (Table 1). The Holocene ^{14}C dates were calibrated using the OxCal v.3.8 program (Ramsey, 2001) based on Stuiver et al. (1998a, b), with a statistical error of 2σ; while the Late Quaternary dates were calibrated according to Bard et al. (1993). Two luminescence (IRSL) age determinations were obtained for the upper kurkar (Table 1) at the TL Laboratory of the Geological Survey of Israel.

Based on the various methods and analyses, the stratigraphic sequences of Cores A and B were divided into 103 and 35 sub-units, respectively. Similarity in properties and clarity of contacts of subsequent sub-units serve as indications for grouping sub-units into 25 and 11 generalized units, respectively (Figs. 3 and 4).

4. Results

The depth of Core A (eastern trough) is 16 and 12 m of Core B (western trough), but the elevation of the bases of both cores is 12 m below sea level (Fig. 2). The two cores are also similar in their general stratigraphy: grayish-brown sandy clay units (Br group), deposited over the kurkar sandstone, and overlain by dark gray–black clay units (GB group) (Fig. 6, Tables 2–4). The thickness of the Br group in Core A is 3.8 m and 2.8 m in Core B whereas the GB group in the eastern trough is much thicker than in Core B: 12.2 m versus 1.7 m thick, respectively (Fig. 6).

The Br units (Fig. 6, Table 4) in both cores are alike in most characteristics: structureless, stiff consistency, sandy-clay texture, low organic matter content, low water content, relatively large amounts of kurkar clasts, and absence of fossils.

The GB units vary in their characteristics within and between the cores but are usually soft, stratified clays

Table 1
Results of radiocarbon and luminescence dating

No.	Core	Sample No.	Depth (m)	Stratig. unit	LAB	Lab no.	C_14 (years BP)	Age BP calibrated (Stuiver et al., 1998a, b)
1	A	AA0	1.90	Aa	ZÜR	ETH-29658	4910±55	5860–5480
2		AA1	2.05	Ab	ZÜR	ETH-29659	4725±55	5590–5320
3		AA8	2.7	Ab	ARZ	AA56737	5202±41	6170–5890
4		AA21	3.9	Ac	ARZ	AA56738	5486±46	6410–6170
5		AA29	4.4	Ad	ZÜR	ETH-28313	6980±65	7940–7670
6		AA34	5.5	Ad	ARZ	AA38933	6293±90	7430–6980
7		A49	6.6	Ae	ARZ	AA38934	6224±70	7290–6900
8		A68	8.6	Aj	ARZ	AA38934	6198±62	7260–6910
9		A73	9.3	Ak	ARZ	AA38936	6783±56	7730–7510
10		A90	10.8	Am	ZÜR	ETH-28314	7765±70	8800–8350
11		A94	11.1	An	ZÜR	ETH-28315	6990±65	7940–7670
12		A102	12.0	Aq	ARZ	AA56735	6768±43	7680–7510
13		A110	13.1	As	ARZ	AA56736	6411±65	7440–7210
14		A121	14.1	Au	ARZ	AA56734	7570±43	8430–8200
15		A128	14.8	Av	ARZ	AA38937	9770±130	11,650–10,650
16		A134	15.4	Ay	ZÜR	ETH-28316	11,500±140	14,000–13,000
17			15.9		GSI	MAM-A	101,000±11,000	
18	B	B1	7.6	Bb	ZÜR	ETH-28317	8170±70	9410–8990
19		B5	7.9	Bd	ARZ	AA38938	7968±51	9010–8640
20		B19	9.2	Bf	ARZ	AA38939	8367±85	9540–9130
21		B29	10.3	Bh	ARZ	AA38940	8515±75	9690–9300
22		B30	10.5	Bi	ARZ	AA38941	9705±70	11,230–10,750
23		B40	11.5	Bj	ZÜR	ETH-28318	19,930±130	20,200–19,650
24			11.9		GSI	MAM-B	59,600±5200	

AMS analyses were performed on the total organic carbon of the sediment.
ARZ: NSF Arizona AMS Laboratory, University of Arizona, Tucson, Arizona.
ZÜR: Institute of Particle Physics, ETH Hönggerberg, Zurich, Switzerland.
GSI: Luminescence Laboratory, Geological Survey of Israel.
Sample nos. 17 and 24 were IRSL dated, and were performed on kurkar sandstone.

with high water content and relatively large amounts of organic material and fossils. The GB group in Core A contains larger amounts of organic matter relative to Core B, 1.5–17.9% versus 2.0–3.2%, respectively, whereas the amount of macro-fossils in Core B is much higher than in Core A.

4.1. Stratigraphy of Core A

The stratigraphic sequence of Core A is presented in Fig. 6 and Table 2. It includes 25 units (Units Ay–Aa). The Br group (Units Ay–Ar) is 3.8 m thick and uncomformably overlies the kurkar sandstone IRSL dated to 101±11 ka. The bottom of this group is radiocarbon-dated to 14,000–13,000 cal. yr BP (Unit Ay), and its top is younger than 7680–7510 cal. yr BP. The grayish-brown units of this group are interbedded with thin, black, soft layers and includes 4 sedimentary cycles each of which is composed of a couplet of 0.8–1.0 m thick grayish-brown Br-type unit (Units Ay, Av, At, Ar) overlain by a thin (up to 0.3 m) black, soft clay layers of GB type (Units As, Au, Aw). The sedimentary cycles (Fig. 6) are: (1) Units Ay–Aw, 1 m thick, (2) Units Av–Au, 0.9 m thick, (3) Units At–As, 1.1 m thick, and (4) Unit Ar, 0.8 m thick. An unconformity between units Ax and Ay may suggest the existence of another possible transition.

The overlying GB group is 12.2 m thick, includes 17 units (Aq–Aa), and the radiocarbon ages range from 7680 to 7510 cal. yr BP (Unit Aq) at the bottom, to 5860–5480 cal. yr BP at the top (Unit Aa). Its uppermost 2 m are disturbed by artificial drainage and agriculture, based on reports, maps and pictures over the last 100 yr (PEF, 1918; Caron, 1922; Schiller, 1979). The sedimentological analysis separates this sequence into 5 sedimentary cycles (Fig. 6): (5) Units Aq–An, 1.1 m thick, (6) Units Am–Aj, 2.6 m thick, (7) Units Ai–Ah, 0.6 m thick, (8) Units Ag–Ae, 1.7 m thick, and (9) Units Ad–Ab, 4.2 m thick. The uppermost unit (Unit Aa) was not divided, since it is disturbed. Typically, each of these cycles is composed of 3–4 sub-units representing various sedimentological characteristics, which were divided into 4 sub-types (Fig. 6, Table 4): (a) silty-sandy unit with low organic matter content (sub-type GB3) at the base of the cycle (cycles 6 and 8), deposited over the top of the previous cycle, (b) an overlying thick (0.7–4.2 m),

Table 2
Stratigraphy, field descriptions, results of laboratory analyses and ages of the sedimentary units of core A (see also Fig. 6)

Depth (m) of upper contact of unit	Cycle no.	Unit no.	Type of unit	No.of sub-units	Thickness of unit (m)	Color	Stiffness	% Water content	% Organic matter	Texture	Content	Structure	Lower bounding surface	Radiocarbon age (cal. yr BP)
0.00		Aa			2.00	Dark gray (5YR4/1)	Soft	33[a]	1.5[a]	Silty clay[a]	Disturbed . not sampled.	Structureless	Gradual	5860–5480
2.00	9	Ab	GB4	3	1.40	Dark gray–black (5YR4/1-5YR2.5/1) with yellowish stains	Soft	33.1	1.5	Silty sand–silty clay	Few kurkar clasts (2–3 mm), few fossil fragments	Structureless	Planar	5590–5320; 6170–5890
3.40		Ac		8	0.60	Dark gray (5YR4/1)	Soft	33.5	2.5	Silty clay	10–20% kurkar clasts (2–15 mm)	Structureless	Gradual??	6410–6170
4.00		Ad		11	2.20	Very dark gray (5YR3.5/1)	Soft	32.4	2.7	Clay–silty clay	Few fossil fragments	Structureless	Erosional plannar	7940–7670; 7,430–6980
6.20	8	Ae	GB2	5	0.80	Very dark gray (5YR3/1)	Soft	39.5	6.3	Silty sand-silty clay	5–10% macro-fossils and vertical trace fossils	Cross-bedding	Gradual	7290–6900
7.00		Af	GB4	6	0.74	Very dark gray (2.5YR3/0) with dark dots	Soft	32.9	4.0	Clay-silty clay	Up to 40% kurkar clasts (2–6 mm), few macro-fossils fragments	Structureless	Lanticular erosional	
7.74		Ag	GB3	1	0.18	Black (2.5YR2.5/0)	Soft	36.1	3.5	Silty sand	Few clasts (<2 mm)	Curved non parallel	Planar erosional	
7.92	7	Ah	GB1	1	0.08	Black (2.5Y2/0)	Frible	39.5	10.2	Clay silt	High quantity of macro-fossils	Laminated	Erosional	
8.00		Ai	GB2	7	0.55	Dark gray–black (7.5YR3.5/0–5YR2.5/1)	Soft	41.6	7.9	Silty clay	Few macro-fossil fragments	Structureless	Planar erosional	
8.55	6	Aj	GB1	1	0.06	Black (5YR2.5/1)	Frible	45.9	17.9	Clay silt[a]	High quantity of macro-fossils	Laminated	Wavy erosional	7260–6910
8.61		Ak	GB4	6	1.22	Very dark gray–black (7.5YR2.5/0–2.5Y2.5/0) with brown stains	Soft	30.6	3.6	Clay–clay silt	5–10% kurkar clasts (5–9 mm); few fossils	Structureless	Wavy erosional	7730–7510
9.83		Al		2	0.70	Very dark gray (7.5YR3/0;5YR3/1)	Soft	33.7	3.2	Clay	10–20% kurkar clasts (2–10 mm); up to 10% macro-fossils	Wavy-curved non-parllel	Erosional (?)	
10.53		Am	GB3	15	0.57	Dark gray–black (7.5YR4/0–10YR2/1)	Soft	36.3	4.7	Sand–silty sand	Up to 10% fossil fragments	Wavy and curved	Planar erosional	8800–8350

11.10	5	An	GB1	1	0.07	Black (7.5YR2/0)	Frible	44.1	12.5	Silty sand		Laminated	Planar erosional	7940–7670
11.17		Ao	GB2	1	0.11	Black (2.5Y2/0)	Soft	27.7	8.6	Silty sand	Few macro-fossil fragments	Curved parallel	Wavy erosional	
11.28		Ap	GB4	4	0.70	Dark gray–very dark gray (7.5YR3/0–10YR4/1), dark vertical veins at the top	Soft	28.3	2.3	Silty clay	Few clasts (<3 mm); piece of wood	Structureless	Lanticular erosional	
11.98		Aq		3	0.20	Very dark gray (7.5YR3/0) at the top, black (7.5YR2/0) at the base	Soft	32.5	2.7	Silty clay		Structureless	Planar erosional	7680–7510
12.18	4	Ar	Br	3	0.82	Very dark gray—very dark grayish brown (10YR3/1.5)	Stiff	20.5	0.5	Sandy clay	Up to 5% clasts (2–5 mm)	Structureless	Erosional	
13.00	3	As	GB4	6	0.34	Very dark gray (10YR3/1) to dark gray (10YR4/1)	Very soft	31.6	4.3	Clay	Up to 10% macro-fossils	Curved non-parallel	Wavy erosional	7440–7210
13.34		At	Br	3	0.78	Very dark grayish brown (10YR3/2)	Stiff	22.1	0.4	Sandy clay	Few clasts (3–6 mm); trace fossils; piece of wood	Structureless	Erosional	
14.12	2	Au	GB2	4	0.01	Alternations of black (7.5YR2/0) and very dark gray (2.5Y3/0; 10YR3/1)	Soft	30.2	6.7	Sand	Few clasts (<3 mm)	Linear cross-bedding	Erosional	8430–8200
14.13		Av	Br	6	0.87	Dark grayish brown (10YR4/2) with black stains and dots	Stiff	19.5	0.2	Sandy clay	Up to 10% clasts (2–8 mm)	Structureless	Planar non-erosional	11,650–10,650
15.00	1	Aw	GB2	1	0.04	Black (2.5YR2.5/0)	Soft	30[a]	6.7[a]	Sand[a]		Structureless	Wavy erosional	
15.04		Ax	Br	2	0.16	Dark gray (10YR4/1; 2.5YR4/0)	Stiff	24.7	0.4	Clay sand	5% kurkar clasts (2–5 mm)	Structureless	Wavy erosional	
15.20		Ay		3	0.80	Dark grayish brown (10YR4/2)	Very stiff	15.0	0.2	Clay sand	Cemented kurkar clasts	Structureless		14,000–13,000
15.90						Very pale brown (10YR7/6)	"Kurkar" sandstone							101 ± 11 ka [b]

[a]Estimation based on similarity of units.
[b]IRSL dates.

Table 3
Stratigraphy, field descriptions, results of laboratory analyses and ages of the sedimentary units of core B (see also Fig. 6)

Depth (m) of upper contact of unit	Cycle no.	Unit no.	Type of unit	No.of sub-units	Thickness of unit (m)	Color	Stiffness	% Water content	% Organic matter	Texture	Content	Structure	Lower bounding surface	Rabdicarbon age (cal. yr BP)
0.00	6	Ba			7.50	Pale yellow (2.5Y7/3)	Friable			Sand			Abrupt, erosional	5100 ± 500[a] (Kadosh et al., 2004)
7.50	5	Bb	tran.	2	0.14	Olive brown (2.5Y4/2)	Soft	36	2.04	Silty sand		Parallel	Lanticular erosional	9410–8990
7.64		Bc	GB5	4	0.24	Dark gray–very dark gray (2.5Y3/0;2.5Y3.5/0)	Soft	36	2.47	Silty sand		Curved parallel	Lanticular erosional	9010–8640
7.88		Bd		2	0.50	Dark gray-very dark gray (2.5Y3.5/0)	Soft	39	2.56	Loam	Up to 30% macro- and trace fossils	Curved	Erosional (?)	
8.38		Be		10	0.72	Dark gray–very dark gray (2.5Y3.5/0;10YR3/1)	Soft	34	3.09	Clay	Up to 90% macro-fossils	Wavy parallel bedding with fossil rich beds	Erosional	
9.10		Bf	tran.	1	0.11	Very dark gray–black (2.5Y2.5/0)	Soft	29	2.89	Silty sand		Structureless	Erosional	9540–9130
9.21	4	Bg	Br	2	0.79	Very dark grayish brown (10YR3/2)	Medium stiff	25	1.16	Silty clay	5–10% kurkar clasts (1–10 mm)	Structureless	Erosional	
10.00	3	Bh	GB5	5	0.37	Very dark gray (2.5YR3/0)	Very soft	35	2.62	Silty clay	Up to 20% macro-fossils	Parallel bedding	Wavy erosional	9690–9300
10.37		Bi	Br	2	0.18	Very dark grayish brown (10YR3/2)	Stiff	29	1.16	Silty clay	5% clasts (< 5 mm); few macro-fossil fragments	Structureless	Wavy erosional	11,230–10,750
10.55	2	Bj		5	1.03	Very dark gray (5YR3/1); dark brown (10YR3/3); dark yellowish brown (10YR4/4)	Stiff	22	0.56	Silty clay-sandy clay	5–30% kurkar clasts (2–7 mm); few macro-fossil fragments	Structureless	Planar erosional	20,000–19,650
11.58	1	Bk		2	0.42	Brown (10YR5/3) to light yellowish brown (10YR6.5/4)	Very stiff	22[a]	0.27	Loam	Cemented kurkar clasts	Structureless		
11.90						Very pale brown (10YR7/6)	"Kurkar" sandstone	59.6 ± 5.2 ka[b]						

[a]Estimation based on simsilarity of units.
[b]IRSL dates.

Table 4
Descriptive and laboratory properties of the various sedimentological sub-types in core A and B

Sub-type	Units	Color	Stiffness	% Water content	% Organic matter	Common texture	Structure	Total thickness of sub-type (m)	% of core
Br type—Cores A & B									
Br(A)	Ay, Ax, Av, At, Ar	Grayish brown	Stiff	20	0.3	Sandy clay; clay–sand	Structureless	3.43	21.5
Br(B)	Bk, Bj, Bi, Bg	Grayish brown–brown	Stiff	25	0.8	Sandy clay; loam	Structureless	2.42	20.1
GB type—Core A									
GB1	Ah, Aj, An	Black	Frible	39.5–45.9	10.2–17.9	Silt–silty sand	Laminar bedding	0.21	1.3
GB2	Ae, Ai, Ao, Au, Aw	Dark gray–black	Soft	27.7–41.6	6.3–8.6	Sand; silty sand; silty clay	Diverse bedding	1.51	9.4
GB3	Ag, Am			36	3.5–4.7	Sand; silty sand	Wavy–curved bedding	0.75	4.7
GB4	Aa-Ad, Af, Ak, Al, Ap, Aq, As			32	3.0	Silty clay–clay	Structureless	10.10	63.1
GB type—Core B									
GB5	Bc–Be, Bh	Dark gray	Very soft	34–39	2.5–3.2	Clay–silty sand	Parellel bedding with macro-fossils	1.83	15.3
Transitional units—Core B									
Bb	Olive brown	Soft	36	2.0	Silty sand	Parallel bedding	0.14	1.1	
Bf	Dark gray–black	Soft	29	2.9	Sand	Structureless	0.11	1.0	
Sand unit—Core B									
Ba	Pale yellow	Frible			Sand		7.50	62.5	

mottled clay unit (GB4 type; cycles 5, 6, 8 and 9), (c) an overlying, organic-rich, silty clay or silty-sandy unit (GB2 type; cycles 5, 7 and 8), and (d) an overtopping unit represented by a thin (6–8 cm) laminated GB1 unit, rich in organic matter (Fig. 6). The upper part of cycle 9 in Core A is disturbed. In general, the texture of each sedimentary cycle is sandier at the base and at the top, while the mid-section is composed of clay. The organic matter content in each cycle increases upsection (Fig. 6).

4.2. Stratigraphy of Core B

The sedimentary sequence of Core B is presented in Fig. 6 and Table 3. It includes 11 units (Units Bk–Ba). The Br group in Core B (Units Bk–Bg) is 2.8 m thick, and uncomformably overlies the kurkar sandstone IRSL dated to 59.6 ± 5.2 ka. The bottom of this group is radiocarbon-dated to 20,200–19,650 cal. yr BP, and the top to 9540–9130 cal. yr BP. One, thin, dark gray soft layer (unit Bh), radiocarbon-dated to 9690–9300 cal. yr BP, is interbedded within the Br sequence. The cycles in Core B are usually separated by unconformities: (1) Unit Bk, 0.4 m thick, (2) Unit Bj, 1 m thick, (3) Units Bi–Bh, about 0.6 m thick, and (4) Unit Bg, 0.8 m thick. The overlying GB group (Units Bf–Bb) is 1.7 m thick, and is younger than 9540–9130 cal. yr BP. The top is radiocarbon-dated to 9010–8640 cal yr BP. The GB group in the western trough (Fig. 6) represents a single cycle (Cycle 5), deposited between about 9540–9130 and 9010–8640 cal. yr BP. This cycle is characterized by gradational textural coarsening and decrease in organic matter content upsection and by large amounts of macro-fossils (GB5 type). The GB group is overlain by a section of 7.5 m friable sand (Unit Ba). This unit (Cycle 6) represents a different sedimentary regime. The unconformity between the sand and the underlying GB unit may suggest a period of exposure and/or truncation of sedimentary units.

4.3. Sedimentology of units

Sedimentological and physical characteristics of all the units are shown in Tables 2 and 3, and Figs. 5 and 6. The Br units are composed of grayish-brown to brown, structureless, stiff, poorly sorted sandy clay, which contains small kurkar clasts (up to 20 mm in size), and very little organic matter (0.3–0.8%). Water content is relatively low at 20–25%. The units lack fossils. The clay assemblage in Core A is composed mainly of smectite and kaolinite, some chlorite and quartz in Core B. The texture of the Br group is clay sand to sandy clay.

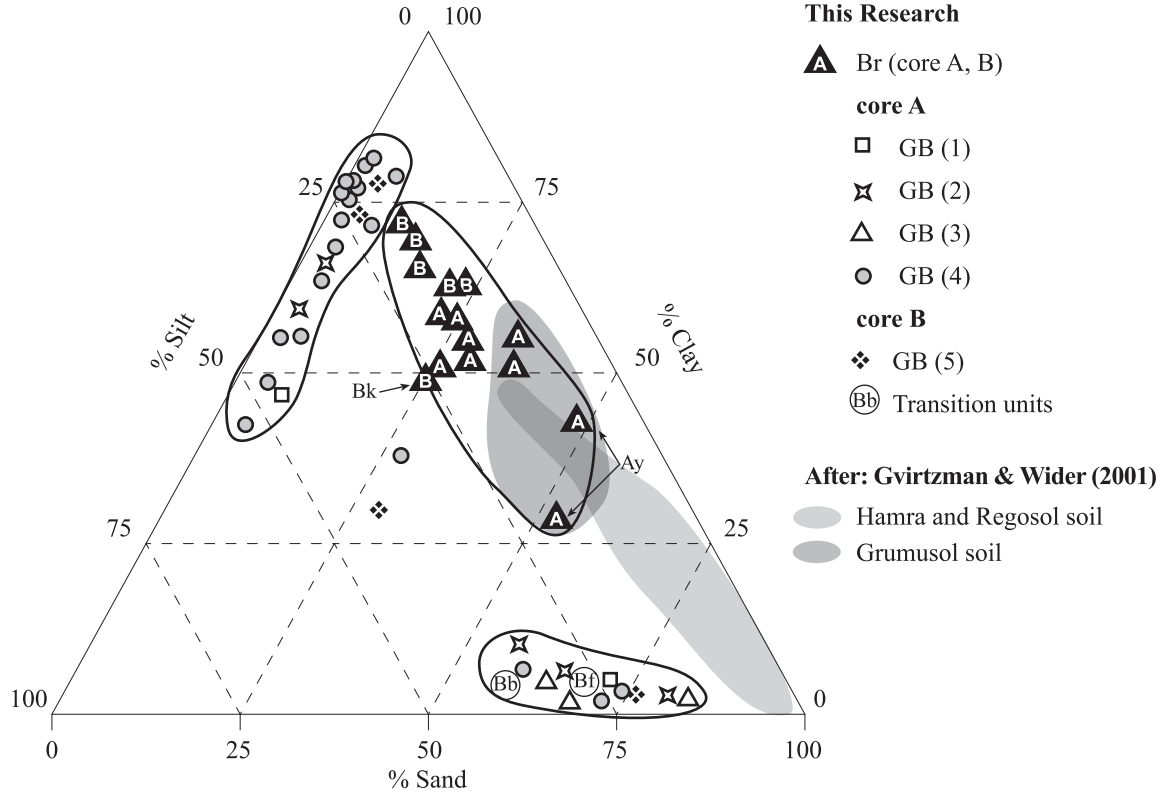

Fig. 5. Texture of Br and GB units in relation to Grumusol and Hamra soils by Gvirtzman and Wieder (2001). Three groups may be observed: (a) the texture of the Br group of Core A resembles the texture of the Grumusol soil and is more sandy than the units of Core B. The lowermost units—Ay and Bk—are more sandy then the overlying Br units. (b) The GB units are organized in two different textural groups. The clay fraction is dominant mainly in GB4 type units. (c) The sand fraction in GB3 type and in the transitional units.

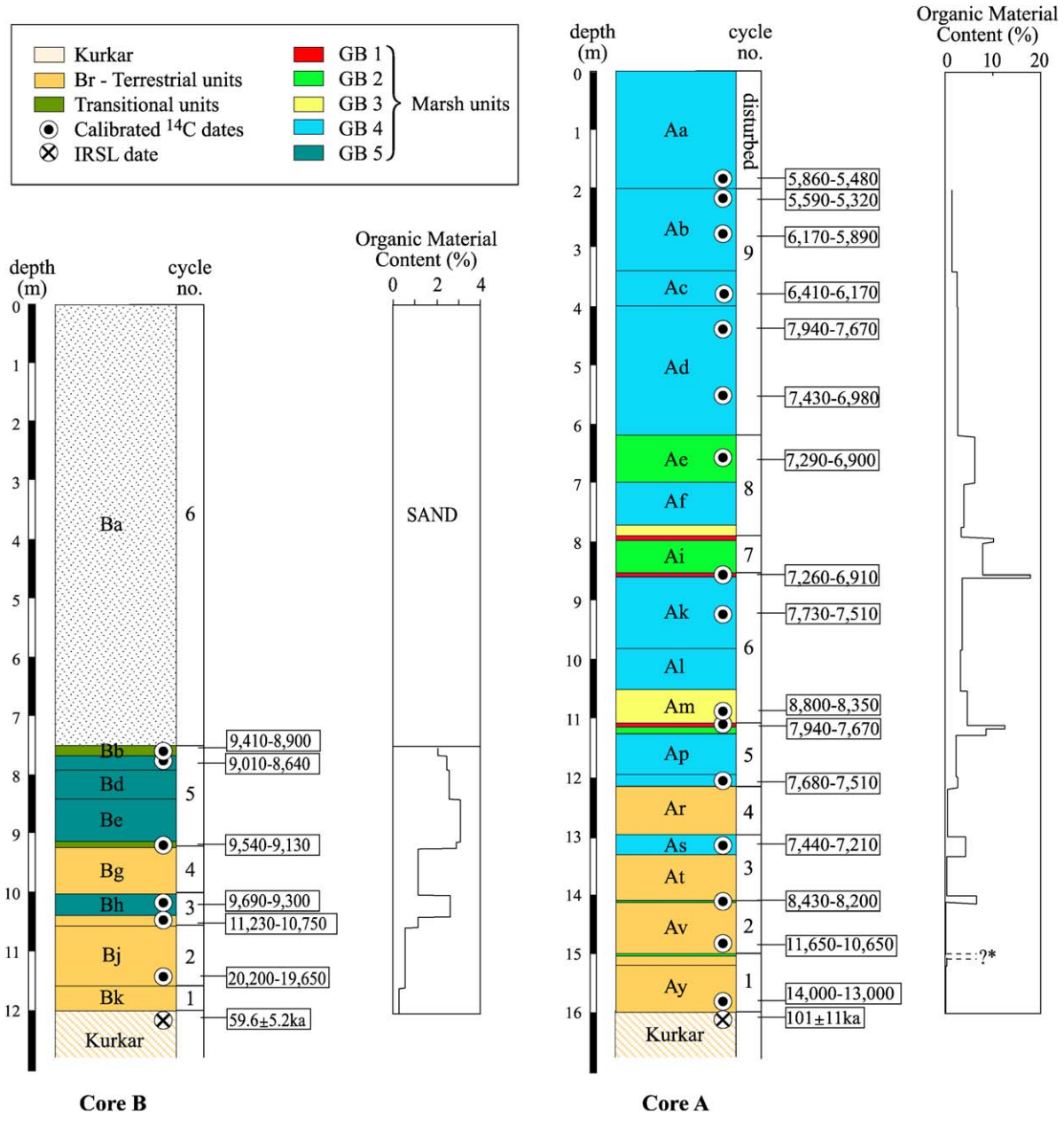

Fig. 6. Stratigraphic columns of Cores A and B including radiocarbon and IRSL ages, sedimentary sub-types, sedimentary cycles and the vertical distribution of organic matter content (see also Tables 2,3).

The GB group is composed of a variety of dark gray–black soft units with silty-sandy or silty clay texture (Fig. 5). The organic matter content varies between 2% and 17.9%, and water content ranges from 27.7% to 45.9%. The GB units are rich in fossils. The sequences were divided into different sub-types according to their field and laboratory characteristics (Table 4). In Core A they are composed of illite–smectite, and differ mainly in organic matter content, texture and structure. Four sub-types were characterized (Table 4, Fig. 5): (1) Sub-type GB1 is friable, laminar, silt to silty-sand in texture, and contains relatively large amounts of organic matter (10.2–17.9%). (2) Sub-type GB2 is silty clay or silty sand in texture, bedded or structureless, and contains 6.3–8.6% organic matter. (3) Sub-type GB3 is composed of wavy or curved silty-sandy units, which contain 3.5–4.7% organic matter. (4) Sub-type GB4 is composed of structureless, silty clay/clay units, mottled with yellowish, brownish and dark stains or dots (probably Mn or Fe,) and contains relatively low amounts of organic matter (1.5–4.0%). All GB sedimentary units in Core B belong to sub-type GB5 (Tables 3,4, Fig. 6). It includes planar to wavy bedded, silty sand units, characterized by a relatively low content of

organic matter (2–3.2%) and macro-fossils (Fig. 4). The clay assemblage includes kaolinite and some chlorite.

Units Bf (11 cm thick) and unit Bb (14 cm thick) in Core B (Fig. 6, Tables 3 and 4) are stratigraphically located between major groups of units: Unit Bf, between the Br group and the overlying GB group, and Unit Bb, between the GB group and the overlying sand. Their sedimentological characteristics show a mix between the overlying and underlying groups, thus they were classified as transitional units.

5. Discussion—interpretation of cores

Cores A and B were located at the deepest part of the eastern and western coastal troughs, respectively, and thus provide the most detailed high-resolution record of the late Pleistocene–Holocene stratigraphy of the Carmel coastal plain. It includes marshy sandy-clay sediments unconformably overlying kurkar sandstone IRSL dated to 101 ± 11 ka in the eastern trough and 59.6 ± 5.2 ka in the western trough. These ages indicate that the durations of the unconformities are about 87,000 yr and less than 40,000 yr, respectively.

5.1. Terrestrial phases

The lower grayish-brown (Br) group which overlies the kurkar in both cores represents a terrestrial phase with deposition of aeolian sand and silt, followed by pedogenesis and formation of soils in an oxidizing environment (Reineck and Singh, 1973; Potter et al., 1980). The lowermost cycles in both cores are sandy in texture. The structureless nature of these deposits maybe related to turbation and mixing processes due to winter-swelling and summer-shrinking of the clays resulting in a uniform clay profile (Wieder and Yaalon, 1983), and/or to compaction and exfiltration of water due to rapid and continuous sedimentation (Reineck and Singh, 1973; Selley, 1976). The low organic matter content of these paleosols (<0.8%) probably represents non-hydric mineral soils (Mitsch and Gosselink, 2000), locally identified as the 'Hamra' soil group, formed over sand and sandstone (Yaalon, 1959). These soils have a finer texture than those of the central coastal plain (Fig. 5; Gvirtzman and Wieder, 2001). The texture of these soils and their low locations at the footslope of the kurkar ridges and in the troughs, suggest that the Br units represent Grumusol soil—a catenary stage of the Hamra soil group (Wieder and Yaalon, 1983). While the origin of the sand fraction of these soils is marine reworked by westerly winds, the origin of the clay fraction of these soils is related to dust fluxes, accumulating in low-topography sites and washed into the sand by intensive pedogenic processes (Gvirtzman and Wieder, 2001).

The Br sequence at the eastern trough is composed of 4 terrestrial cycles of relatively thick sandy clay soils truncated by floods which deposited thin dark clay units. The terrestrial phase at the eastern trough lasted about 6000 yr, from 14,000–13,000 cal. yr BP until about 7680–7510 cal. yr BP (Fig. 6).

The terrestrial phase in the western trough is longer and started prior to 20,200–19,650 cal. yr BP, and continued until 9540–9130 cal. yr BP—more than 11,000 yr. The Br sequence includes also 4 cycles but their texture is slightly finer (Fig. 5). The ages show that the Br units in both cores were deposited from the Late Pleistocene, and continued to accumulate during the early Holocene. The uppermost cycle of the Br group in both cores is unconformably overlain by the GB group sequence indicating abrupt change into marsh environment. These marshes were not synchronous, and part of the time terrestrial conditions at the eastern trough paralleled marsh environment at the western trough.

5.2. The marsh phases

The upper part of both cores consists of dark gray–black units (GB group) that represent a sequence of fine-grained sediments deposited in a marshy environment.

In the eastern trough these units show characteristics of calcareous hydromorphic soils, identified as mineral soils in a reducing environment (Yaalon, 1959). The dark color of these sediments is related to the high organic content, and/or reduction processes under a shallow water cover (Reineck and Singh, 1973). The relatively large amounts of organic material found in these units (Fig. 6) indicate a marsh environment with intensive vegetation. At the eastern trough, this phase started at about 8100 to 7500 cal yr BP (Fig. 6) and continued up to the present, but more than 80% of the section was deposited before 5860–5480 cal. yr BP, about 2000 yr. Similar radiocarbon ages, 7360–7240 cal. yr BP at a depth of about 8 m, were obtained by Chomicki (2002) (Core 17; Fig. 1). The eastern marsh complex includes five sedimentary cycles interpreted as five generations of marshes. Each marsh cycle is characterized by coarser texture and low amounts of organic matter (3.5–4.7%) at the base of the cycle, indicating sand incursion which buried the previous marsh. These units are overlain by a structureless, clay sub-unit mottled with Mn and Fe concentrations typical of a reducing environment, which contains a very low amount of organic material (up to 3.3%). Such characteristics indicate hydromorphic mineral soil subjected to alternations of wetting and drying during seasonal flooding and shallow water cover (Mitsch and Gosselink, 2000). The lack of structure may result from rapid sedimentation and pedogenesis (Reineck and Singh, 1973; Selley, 1976). It is overlain by a wavy/

cross-bedded sub-unit caused by various flow rates (Davis, 1983), which also contains increasing amounts of organic material (6.3–8.6%), and trace fossils (Bouma, 1963), which indicate relatively intensive vegetation cover, reflecting deepening of the water and further development of the marsh. The overtopping unit in each cycle has a relatively high content of organic matter (up to 17.9%). This high organic matter content and the clay texture represent organic-rich mineral soil in a shallow and relatively stable marsh environment (Mitsch and Gosselink, 2000). The laminar bedding of this unit is probably the result of sorting by suspension in a calm water body (Reineck and Singh, 1973; Davis, 1983).

At the western trough the marsh phase was relatively short—about 900 yr, as indicated by the deposition of the GB units from 9540–9130 cal. yr BP to 9010–8640 cal. yr BP. The clay units deposited during this phase show little evidence of pedogenesis, which suggests a more permanent water cover. The parallel bedding indicates deposition of fine particles in constant water-cover with changes of water depth. The low organic matter content (2–3.2%) implies less vegetation cover in this marsh, maybe because of the high salinity values of the water, as indirectly presented by the macro-fossil assemblage within the sediments, typical of a brackish water environment. Galili and Weinstein-Evron (1985) claimed that the coastal marshes were brackish, based on pollen analyses and botanical remains. They suggested that the northern Carmel coastal marshes were a series of fresh-water to slightly brackish swamps, with decreasing salinity to the south. In Dor, the faunal assemblage indicates low salinity to brackish water (Sivan et al., 2004b), as was also indicated by Sneh and Klein (1984). The dating shows that at the time when marshes prevailed at the western trough, terrestrial conditions predominated at the eastern trough and continued even when the marshes at the west completely dried up. The eastern marshes were formed only about 1000 yr later.

The overlying sand in the western trough is probably aeolian. The unconformity between the sand and the underlying GB unit suggest a period of exposure and/or truncation of sedimentary units. The base of the sand was IRSL dated to 5100 ± 500 yr in Dor (Kadosh et al., 2004), and accumulated since then, burying the dark clays after being exposed for more than 3500 yr, during which Pre-Pottery Neolithic and chalcolithic settlements existed.

During the 3rd century the marshes of the eastern trough were turned into an artificial reservoir by the Roman and Byzantine dams (Porath, 2002), and the shallow water level of the natural marshes was raised by about 2 m. The shallow water cover returned during the 13th century when Caesarea was abandoned (Chomicki, 2002). The base of the reservoir deposits varies in depth from 2 to 6 m, and exceeds 3.3 m in Core 17 (Chomicki, 2002), located 0.5 km southeast of the present study site (Fig. 1).

6. The palaeoenvironment of the southern Carmel coastal plain

The Carmel coastal plain topography consists of north–south late Pleistocene kurkar ridges. The troughs between the ridges preserve evidence of terrestrial phases of sand and loess deposition, and intensive pedogenesis of local brownish hamra soils during the late Pleistocene and Holocene. This phase is followed by an abrupt environmental change, in which marsh covered the troughs, and dark clays were deposited during the Holocene. In the western trough an unconformity after the marsh phase represents an exposure time of several thousand years, and later on burial by a thick aeolian sand cover.

6.1. Terrestrial phase —20,200–19,650 to 14,000–13,000 cal. yr BP

During this phase sand and loess were deposited and brown Grumusol soils of the Hamra Group developed in the western trough. The minimum rate of accumulation during this period was relatively low, 0.01–0.02 cm/yr These low rates of sand and loess fluxes into the coastal plain may be related to the location of the coastline, over 8 km to the west, and the relatively wet climate conditions (Gvirtzman and Wieder, 2001). Hamra soil formation between 20 and 12 ka along the Carmel coastal plain was also documented by Frechen et al. (2004) indicating relatively wetter conditions (Yaalon and Dan, 1967). In Dor to the north, correlative units, dated to between 26,000 and 12,000 cal. yr BP, do not contain any pollen grains (Kadosh et al., 2004), and therefore, no direct palaeoclimatic interpretation can be deduced.

Comparing our data to paleoclimatic evidence, such as the speleothem records (Fig. 7), suggests that the lower Grumusol soils started to develop at the western trough in cold and dry climatic conditions, with the minimum ages between 20 and 17 ka, corresponding to the LGM (Bar-Matthews et al., 1997a, 1998, 1999; Frumkin et al. 1999, 2000; Vaks et al., 2003). The eastern trough was exposed from sedimentary cover, probably, by the fluvial activity of the streams flowing to a base level 120 m lower at a gradient of about 0.01 m/m. Only little accumulation took place at the western trough. Lake Lisan (the precursor of the present-day Dead Sea) levels exceeded their maxima at 165 m below sea level between 26 and 23 cal. ka BP (Bartov et al., 2002). These high levels were interpreted as indicative of wetter conditions resulting from an increase in the

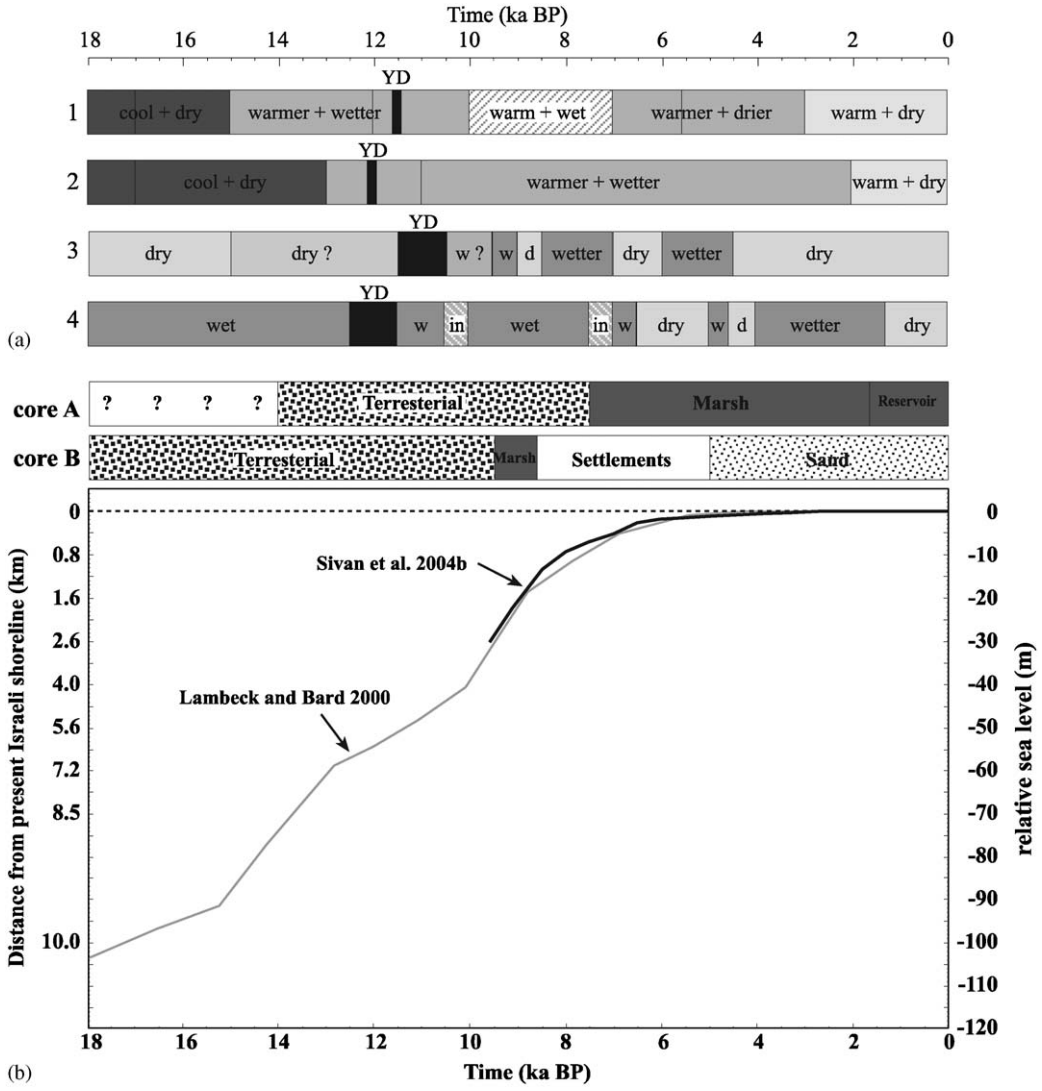

Fig. 7. (a) Relative sea-level—between 18 and 9.5 ka BP after Lambeck and Bard (2000); between 9.5 ka BP and the present, after Sivan et al. (2004b); distance from present coastline from −120 to −50 m below present sea-level is calculated after Israel Ports Authority (1987), and between –50 and present sea-level after Oceana Marine Research (1999). Paleoenvironments in the study area represented in Cores A and B. (b) Comparative palaeoclimatic records in Israel: (1) Continental isotopes from speleothems, Soreq Cave (Bar-Matthews et al., 1997a, b, 1998, 1999). (2) Continental isotopes from speleothems in Jerusalem Caves (Frumkin et al., 1999, 2000). (3) Lake Lisan levels—18–15 ka BP after Bartov et al. (2002); 15–9.5 ka BP after Begin et al. (1985) and Yechieli et al. (1993, 1998); Dead Sea levels from 9.5 ka BP to present (Enzel et al., 2003). (4) Sand deposition and pedogenesis along the coastal plain after Gvirtzman and Wieder (2001).

multiyear average annual precipitation (Enzel et al., 2003). Between 23 and 17 cal. ka BP the lake Lisan level dropped to 225 m below mean sea level (Bartov et al., 2002), indicating a drier climate towards and during the LGM. The fall of the Dead Sea level continued, and reached about 300 m below mean sea level at about 15 cal. ka BP (Bartov et al., 2002; Fig. 7). This post-glacial period was correlated to the cold arid North Atlantic Heinrich event H1 (Bartov et al., 2003). Gvirtzman and Wieder (2001) indicated that, generally a relatively wetter climate prevailed along the coastal plain between 40 and 12.5 cal. ka BP, during which red Hamra soils developed. Between 17 and 15 ka (Bar-Matthews et al., 1997a, 1998, 1999), or between 17 and 13 ka (Frumkin et al., 1999, 2000), climate was still cool and dry, but with a gradual trend of warming and increasing precipitation, until about 12 ka (Fig. 7).

6.2. Terrestrial phase —14,000–13,000 to 9540–9130 cal. yr BP

During this period sand and loess were deposited in both troughs and brown Grumusol soils developed. The minimum rate of accumulation from about 11 cal. ka BP

to the early Holocene increased dramatically up to 0.1 cm/yr considering erosion but no significant compaction due to the lack of organic matter and the high portion of sand. This trend can be attributed to (a) relatively quick sea-level rise from −75 to about −25 m (Fairbanks, 1989; Lambeck and Bard, 2000) and coastline transgression from about 8.5 to 2.3 km (Israel Ports Authority, 1987; Fig. 7), which provided increasing sand potential; and (b) increased dust deposition indicating wetter conditions (Gvirtzman and Wieder, 2001). Frechen et al. (2002) documented Hamra soil formation between 15 and 12 ka. In general, between 15 and 10 ka (Bar-Matthews et al., 1997a, 1998), or between 13 and 11 ka (Frumkin et al., 1999, 2000), warmer and wetter conditions prevailed excluding the cold and arid Younger Dryas at around 11.5 ka.(Bar-Matthews et al., 1997a; Frumkin et al., 2000, 2001). The pollen assemblage in Dor between 12 and 10 cal. ka BP also indicates dry and cool conditions (Kadosh et al., 2004). This dramatic event caused an extreme drop of the Lake Lisan level between about 11.5 and 10.5 ka (noncalibrated, Neev and Emery, 1967; Begin et al., 1985; Yechieli et al., 1993, 1998; Fig. 7). Gvirtzman and Wieder (2001) documented a thick layer of loess deposited along the coastal region of Israel during the Younger Dryas (12.5–11.5 cal. ka BP). They estimated the rate of deposition during this period at 0.07 cm/yr

In contrast to the above palaeoclimaic studies, no indication of the Younger Dryas event was recorded in our study area. Sand, loess and brown soils accumulated continuously until 9540–9130 cal. yr BP in the western trough, and up to 8100–7500 cal. yr BP in the eastern trough.

6.3. West marshes—asynchronous period (I)—9540–9130 to 9010–8640 cal. yr BP

An abrupt environmental change occurred in the study area, and a wetland developed in the western trough (Fig. 7), depositing dark clays. Sedimentation rates for this short-lived (about 900 yr) marsh are relatively low, about 0.18 cm/yr, compared to the eastern marshes. At the same time at the eastern trough, brown Grumusol soils continued to accumulate. The palynological data from Dor suggests wetter conditions between 10,300 and 9500 cal yr BP (Kadosh et al., 2004).

Following the Younger Dryas the Dead Sea level tended to rise, and exceeded an elevation >370 m below mean sea level at about 9000 cal. yr BP (Enzel et al., 2003). Warm and wet conditions for the Early Holocene—between 10 and 7 ka were interpreted from the cave records (Bar-Matthews et al., 1997a, 1998; Frumkin et al., 1999, 2000). Bar-Matthews et al. (2000) correlated this period to the humid phase of Sapropel 1 evident in the palynological analyses of the eastern Mediterranean (Rossignol-Strick, 1999). Lacustrine sequences were deposited between 10.3 and 8.0 cal. ka BP (Frumkin et al., 2001) in the Dead Sea, indicating a deeper lake and a relatively wetter climate. Between 11.5 and 7.5 cal. ka BP, Gvirtzman and Wieder (2001) show alternations between periods of soil formation, indicating wetter conditions, and periods of sand accumulation, representing drier conditions (Fig. 7).

The marsh phase at the western trough parallels the second deglaciation phase (melt-water pulse 1B) which started at about 9500 BP (Fairbanks, 1989). The sea level along the Israeli coast, at the beginning of the Holocene, is estimated between 20 and 25 m below the present level (Galili et al., 1988; Sivan et al., 2001, 2004b) and at about −40 m by Lambeck and Bard (2000). During this short marsh cycle at the western trough sea level rose from −25 to about −15 m and the reconstructed location of the coastline was between about 2.3 and 1 km west of that at present (Oceana Marine Research, 1999; Fig. 7).

6.4. Drying of the western marshes—asynchronous period (II)—9010–8640 cal. yr to 5100 yr

The western marshes dried up in the study area at about 9010–8640 cal. yr BP (Fig. 7). At other sites along the Carmel coast the marshes dried even earlier, between 10,000 and 8600 cal. yr BP (Kadosh et al., 2004; Sivan et al, 2004a). All Pre-Pottery Neolithic settlements (Galili and Nir, 1993), and also later Neolithic and Chalcolithic sites along the Carmel coast (Raban, 1983; Galili and Weinstein-Evron, 1985), were settled on top of the dark clays deposited by these marshes. The marsh sediments, with the various settlements over it were covered by sand (Fig. 7) since about 5100 yr (Kadosh et al., 2004), providing an exposure time of about 3600 yr. These findings show that the marshes along the Carmel coast prevailed at the beginning of the Holocene for several hundred years before drying out, in spite of sea-level rise. The abrupt initiation of the marshes while the coastline was far to the west (about 2.3 km), and their drying up while the coastline was about 1 km to the west, may suggest that sea-level rise is not the only cause for wetland initiation or termination.

In general, the period between 7000 and 3000 yr BP was warmer and wetter than at present, but with a trend towards aridity (Bar-Matthews et al., 1997a, b, 2003; Frumkin et al., 1999; Fig. 7). Large fluctuations of Dead Sea levels between about 415 and 360 m below mean sea level between about 8500 and 4500 cal. yr BP (Fig. 7) were documented by Enzel et al. (2003), Kadan (1996) and Frumkin et al. (2001), indicating major fluctuations in precipitation during the early and middle Holocene. Nevertheless, for about 70% of this time span Dead Sea levels were rising or stationary at high levels indicating relatively wetter conditions. The eastern (Kabara) marshes, initiated about 1000 yr after the western

marshes dried paralleled the exposure period from 7680 to 7510 cal. yr BP

6.5. *Kabara (Eastern) marshes—asynchronous period (III)—7680–7510 cal. yr BP to present*

The Kabara marshes were initiated at about 7680–7510 cal. yr BP. The succession shows short episodes of drying and/or burial of vegetation-rich marshes by aeolian sand fluxes. These shallow water marshes (Chomicki, 2002) existed until the present, but since the 3rd century the natural marsh was converted into an artificial reservoir about 2 m deep.

The sedimentation rates at the marshes between about 7600 and 5600 cal. yr BP were high: 10 m of sediments were deposited during a period of about 2000 yr (Fig. 7), a sedimentation rate of about 0.5 cm/yr. The sediments are mainly continental clays transported by floods from the east, and aeolian sand pulses from the sea side. Sand accumulation between 7 and 5 ka was documented by Frechen et al. (2002) in the Sharon coastal plain south of the Carmel coast. These amounts of fluvial sediments can be explained by a higher frequency of large floods related to higher rainfall intensities and/or higher annual rainfall amounts. The marsh cycles during this period suggest fluctuations in type and amounts of sediments, possibly related to climate fluctuations typical of the mid- and late Holocene (Fig. 7). Sedimentation rate since about 5600 cal. yr BP decreased dramatically to 0.036 cm/yr. Alternations between sand accumulation and initial pedogenesis in the coastal plain since 7500 cal. yr BP were documented by Gvirtzman and Wieder (2001). Dead Sea levels between about 7000 and 6000 cal. yr BP fell from about 360 to 415 m below mean sea-level (Enzel et al., 2003) indicating drier conditions and rose again to about 370 m below mean sea level at about 5000 cal. yr BP. representing wetter climate. Since about 3000 cal. yr BP the climate has become warmer and drier (Bar-Matthews et al., 1997a, b, 2003; Frumkin et al., 1999; Fig. 7). Mediterranean Sea level at 7500 yr BP was already at about –5 m, and less than 0.5 km from the present shoreline. This proximity must have had at least an indirect effect on the formation of the Kabara marshes possibly through groundwater level rise resulting from rising sea level.

6.6. *Sand cover—western trough—asynchronous period (IV)—from 5100 yr to present*

The sand started to accumulate at the western trough at about 5100 yr in response to a sea-level rise to a 1–2 m below its present level. The coastline location was some tens to hundreds of meters distant of the present (Galili et al., 1988; Sivan et al., 2001, 2004b). Aeolian sand accumulation since 5 ka was documented by Frechen et al. (2002) in the Sharon coastal plain. Only during the Middle Bronze IIA (about 4000 BP) did people start to settle on the exposed kurkar ridges (Raban and Galili, 1985), as represented at Dor (Stern, 1993). Continuous settlement on the kurkar ridge from 4000 yr BP during the Crusader period (about 700 yr BP) until present indicates that the sea was somewhere close in the west and marshes prevailed in the east.

7. Conclusions

(a) The Late Pleistocene–Holocene sedimentary sequences in the western and eastern troughs of the southern Carmel coastal plain unconformably overlie Pleistocene kurkar sandstone, and include two major sedimentary units: (I) brown sandy clay Grumusol soil of the 'Hamra' soil group, indicating terrestrial conditions of aeolian deposition of marine reworked sand, aeolian dust and intensive pedogenic processes in a well-drained, oxidizing environment, and (II) an overlying sequence of dark silty clay sediments, indicating wetland conditions of fresh to brackish, shallow-water marsh with organic-rich, mineral, hydromorphic soils.

(b) The terrestrial phases prevailed between 20,200–19,650 and 9540–9130 cal. yr BP in the western trough, and between 14,000–13,000 and 7680–7510 cal yr BP in the eastern trough. Sequences in both cores were divided into 4–5 depositional cycles separated by unconformities or by different deposits. These phases are generally related to the gradual warming and wetter climate after the LGM, causing an increased loess deposition. The sea level was steeply rising causing an increasing rate of sand influx while the coastline was still far to the west (between 10.5 and 2.3 km).

(c) The marshes in the troughs were asynchronous: the eastern marshes postdate the western marshes by about 1000 yr. The marshes differ in their properties, such as water quality, amount of vegetation cover and fauna. These differences probably indicate different generative mechanisms. The short-lived western marshes were formed while coastline was about 2.3 km west of present, prevailed between 9540–9130 and 9010–8640 cal. yr BP (about 900 yr), and then dried up while the shoreline was about 1 km to the west. The marsh sediments at the western trough were exposed for about 3600 yr, during which Pre-Pottery Neolithic to Chalcolithic settlements existed while the coastline was transgressing eastward from about 1 to 0.5 km. The causal factor of this short but regional event is rather unclear. The entire trough was covered by sand resulting from the rising sea level from about 5100 yr BP. The Kabara marshes at the eastern trough prevailed from 7680–7510 cal. yr BP until present.

The sequence consisted of 5 short marsh episodes, each of which was estimated at few hundred years, within about 2000 yr. Each cycle buried the previous marsh with sand before it produced a vegetation-rich marsh. The genesis of these marshes is related to the following factors: (I) climate was warmer and wetter than at present, but with a gradual trend towards aridity. This trend was reflected in an increased frequency of large floods at the streams which drain into the marshes, and relatively high sedimentation rates of up to 0.66 cm/yr; and (II) the rise of groundwater level resulting from sea-level rise almost to the present level.

Acknowledgments

This research was funded by grants from: Sir Maurice and Lady Hatter Fund of the Recanati Institute for Maritime Studies (RIMS), the Frenkel Family Fund of the Haifa and Galilee Research Center, University of Haifa Research funds. We thank Dr. G. Bonani of the Institute of Particle Physics, Zurich, Switzerland, and Dr. N. Porat of the Israel Geological Survey, Jerusalem, for the dating analyses. The authors thank Noga Yoselevich for the figures. This manuscript forms a portion of Ronit Cohen-Seffer's doctorial dissertation supervised by Dorit Sivan, Noam Greenbaum and Moshe Inbar, at the University of Haifa.

References

Almogi-Labin, A., Schilman, B., Perelis-Grossowicz, L., 2002. The brackish-water foraminifera of the inland Enot Timsah Ponds, Mount Carmel coastal plain, Israel. Geological Survey of Israel Current Research 13, 79–85.

Bard, E., Maurice, A., Fairbanks, R.G., Hamelin, B., 1993. ^{230}Th–^{234}U and ^{14}C ages obtained by mass spectrometry on corals. Radiocarbon 35 (1), 191–199.

Bar-Matthews, M., Ayalon, A., Kaufman, A., 1997a. Late Quaternary paleoclimate in the eastern Mediterranean region from stable isotope analysis of speleothems at Soreq Cave, Israel. Quaternary Research 47, 155–168.

Bar-Matthews, M., Ayalon, A., Kaufman, A., 1997b. Middle to late Holocene (6,500 yr. period) paleoclimate in the Eastern Mediterranean region from stable isotopic composition of speleothems from Soreq Cave, Israel. In: Issar, A., Brown, N. (Eds.), Water, Environment and Society in Times of Climatic Change. Kluwer Academic Publishers, Netherlands, pp. 203–214.

Bar-Matthews, M., Ayalon, A., Kaufman, A., 1998. Paleoclimate evolution in the Eastern Mediterranean region during the last 58,000 years as derived from stable isotopes of speleothems (Soreq Cave, Israel). In: Isotope Techniques in the Study of Environmental Change, Proceedings of International Symposium, Vienna, 14–18 April 1997. International Atomic Energy Agency, Vienna, pp. 637–682.

Bar-Matthews, M., Ayalon, A., Kaufman, A., Wasserburg, G.J., 1999. The Eastern Mediterranean paleoclimate as a reflection of regional events: Soreq Cave, Israel. Earth and Planetary Science Letters 166, 85–95.

Bar-Matthews, M., Ayalon, A., Kaufman, A., 2000. Timing and hydrological conditions of Sapropel events in the Eastern Mediterranean, as evident from speleothems, Soreq Cave, Israel. Chemical Geology 169, 145–156.

Bar-Matthews, M., Ayalon, A., Gilmouru, M., Matthews, A., Hawkesworth, C.J., 2003. Sea–land oxygen isotopic relationships from planktonic foraminifera and speleothems in the eastern Mediterranean region and their implication for palaeorainfall during interglacials. Geochimica and Cosmochimica Acta 67 (17), 3181–3199.

Bar-Yosef, O., 1998. Prehistory chronology for the Holy land. In: Levy, T.E. (Ed.), The Archaeology of Society in the Holy Land. Preface XV. University Press, Leicester, London.

Bartov, Y., Stein, M., Enzel, Y., Agnon, A., Reches, Z., 2002. Lake levels and sequences stratigraphy of Lake Lisan, the late Pleistocene precursor of the Dead Sea. Quaternary Research 57, 9–21.

Bartov, Y., Goldstein, S.L., Stein, M., Enzel, Y., 2003. Catastrophic arid episodes in the Eastern Mediterranean linked with the North Atlantic Heinrich events. Geology 31 (5), 439–442.

Begin, Z.B., Broecker, W., Druckman, Y., Kaufman, A., Magaritz, M., Neev, D., 1985. Dead Sea and Lake Lisan levels in the last 30,000 years: a preliminary report. Israel Geological Survey Report 29/85, 1–18.

Broshi, M., Gophna, R., 1986. Middle Bronze Age II Palestine: its settlements and population. Basor 261, 73–90.

Bouma, A.H., 1963. A graphic presentation of the Facies Model of salt marsh deposits. Sedimentology 2, 122–129.

Campell, J.B., 1996. Introduction to Remote Sensing. Taylor and Francis, London.

Caron, L., 1922. Project D'Assainissement et D'Irrigation des Terrains de Kabbara. Jewish Colonization Association-Commission Palestinienne, Dijon.

Chomicki, K., 2002. The paleoevolution of the ancient reservoir of Caesarea. M.Sc. thesis, McMaster University, Hamilton, Ontario.

Collinson, J.D., Thompson, D.B., 1989. Sedimentary Structures. Unwin Hyman, London.

Davis Jr., R.A., 1983. Depositional Systems. Prentice-Hall, New Jersey 669pp.

Enzel, Y., Bookman (Ken Tor), R., Sharon, D., Gvirtzman, H., Dayan, U., Ziv, B., Stein, M., 2003. Late Holocene climates of the Near-East deduced from Dead Sea-level variations and modern regional winter rainfall. Quaternary Research 60, 263–273.

Fairbanks, R.G., 1989. A 17,000-years glacio-eustatic sea-level record: influence of glacial melting rates on the Younger Dryas event and deep ocean circulation. Nature 342, 637–642.

Frechen, M., Neber, A., Dermann, B., Tsatskin, A., Boenigk, W., Ronen, A., 2002. Chronostratigraphy of aeolianites from the Sharon Coastal Plain of Israel. Quaternary International 89, 31–44.

Frechen, M., Neber, A., Dermann, B., Tsatskin, A., Boenigk, W., Ronen, A., 2004. Chronostratigraphy of Pleistocene sedimentary cycles in the Carmel Coastal Plain of Israel. Quaternary International 121 (1), 41–52.

Frumkin, A., Ford, D.C., Schwarcz, H.P., 1999. Continental oxygen isotopic record of the last 170,000 years in Jerusalem. Quaternary Research 51, 317–327.

Frumkin, A., Ford, D.C., Schwarcz, H.P., 2000. Paleoclimate and vegetation of the last glacial cycles in Jerusalem from a spelothem record. Global Biogeochemical Cycles 14 (3), 863–870.

Frumkin, A., Kadan, G., Enzel, Y., Eyal, Y., 2001. Radiocarbon chronology of the Holocene Dead Sea: attempting a regional correlation. Radiocarbon 43, 1179–1189.

Galili, E., Weinstein-Evron, M., 1985. Prehistory and palaeoenvironments of submerged sites along the Carmel Coast of Israel. Paléorient 11 (1), 37–51.

Galili, E., Weinstein-Evron, M., Ronen, A., 1988. Holocene sea-level changes based on submerged archaeological sites off the Northern Carmel Coast in Israel. Quaternary Research 29, 36–42.

Galili, E., Nir, Y., 1993. The submerged Pre-Pottery Neolithic water well of Atlit-Yam, Northern Israel, and its paleoenvironmental implications. The Holocene 3 (3), 265–270.

Garfinkel, Y., 1999. Neolithic and chalcolithic pottery of the southern Levant. In: Belfer-Cohen, A., Foerster, G., Stern, E., Tsafrir, Y. (Eds.), Qedem, Monographs of the Institute of Archaeology, vol. 39. The Hebrew University of Jerusalem, pp. 306–313.

Gophna, R., Portugali, Y., 1988. Settlement and demographic processes in Israel's coastal plain from the Chalculithic to the Middle Bronze Age. Basor 269, 11–28.

Guttman, J., 1998. Defining flow systems and groundwater interactions in the multi-aquifer system of the Carmel Coast region. Ph.D thesis, Tel Aviv University, Mekorot Report No. 467.

Gvirtzman, G., Wieder, M., 2001. Climate of the last 53,000 years in the Eastern Mediterranean, based on soil-sequence stratigraphy in the coastal plain of Israel. Quaternary Science Reviews 20, 1827–1849.

Inbar, M., Sivan, D., 1984. Paleo-urban development and Late Quaternary environmental change in the Akko area. Paléorient 9/2, 85–91.

Israel Ports Authority (IPA), 1987. Bathymetric map of the coast of Israel between Rosh Hanikra and Tel Aviv, 1:100,000 scale.

Kadan, G., 1996. Evidence of Dead Sea lake level fluctuations and recent tectonism from the Holocene fan-delta of Nahal Darga. M.Sc. thesis, Ben-Gurion University of Beer-Sheva (in Hebrew, English abstract).

Kadosh, D., Sivan, D., Kutiel, H., Evron-Weinstein, M., 2004. Late Quaternary environmental changes based on stratigraphy and palynological data obtained from Dor, Carmel coast, Israel. Palynology 28, 143–157.

Lambeck, K., Bard, E., 2000. Sea-level change along the French Mediterranean coast since the time of the Last Glacial Maximum. Earth and Science Planetary Letters 175, 203–222.

Michelson, H., 1970. The geology of the Carmel coast. M.Sc. thesis, The Hebrew University, Jerusalem and Tahal, Tel Aviv, HG/70/025, 60pp. (in Hebrew).

Mitsch, W.J., Gosselink, J.G., 1993. Wetlands. Van Nostrand Reinhold, New York.

Mitsch, W.J., Gosselink, J.G., 2000. Wetlands. Wiley, New York.

Mülinen, H., 1907. Beiträge zur Kenntnis des Karmels. Manuscript, Privately published.

Neev, D., Emery, K.O., 1967. The Dead Sea: Depositional Processes and Environments of Evaporates. Israel Geological Survey Bulletin 41.

Orme, A.R., 1991. Wetland morphology, hydrodynamics and sedimentation. In: Williams, M. (Ed.), Wetlands—A Threatened Landscape. Basil Blackwell, Oxford, pp. 42–94.

Oceana Marine Research (OMR), 1999. Bathymetric chart of the coast of Israel, 1:20,000 scale.

Palestine Exploration Fund (PEF), 1918. Map, scale 1:63,000. Palestine Exploration Fund.

Porath, Y., 2002. The water-supply to Caesarea: a re-assessment. In: Amit, D., Patrich, J., Hirschfeld, Y. (Eds.), The aqueducts of Israel. Journal of Roman Archaeology Supplement 46, 103–129.

Potter, P.E., Maynard, J.B., Pryor, W.A., 1980. Sedimentology of Shale. Springer, New York.

Raban, A., 1983. Recent maritime archaeological research in Israel. International Journal of Nautical Archaeological Underwater Explorations 12, 229–251.

Raban, A., 1987. Alternated river courses during the Bronze Age along the Israeli coastline. Colloques Internationaux C.N.R.S. deplacements des lignes de rivage en Mediterranee, Paris.

Raban, A., Galili, E., 1985. Recent maritime archaeological research in Israel—a preliminary report. International Journal of Nautical Archaeology 14 (4), 321–356.

Ramsey, B.C., 2001. Development of the Radiocarbon Program OxCal. Radiocarbon 43 (2A), 355–363.

Reineck, H.E., Singh, I.B., 1973. Depositional Sedimentary Environments. Springer, Berlin.

Rossignol-Strick, M., 1999. The Holocene climatic optimum and pollen records of Sapropel 1 in the Eastern Mediterranean, 9,000–6,000 BP. Quaternary Science Reviews 18, 515–530.

Schiller, E., 1979. The First Photographs of the Holy Land. Ariel Publication House, Jerusalem 380pp.

Schumacher, G., 1887. Research in the Plain North of Caesarea. Palestine Exploration Fund—Quarterly Statement for 1887, London, pp. 78–90.

Selley, R.C., 1976. An Introduction to Sedimentology. Academic Press, London.

Sivan, D., Gvirtzman, G., Sass, E., 1999. Quaternary stratigraphy and paleogeography of the Galilee coastal plain, Israel. Quaternary Research 51, 280–294.

Sivan, D., Wdowinsky, S., Lambeck, K., Galili, E., Raban, A., 2001. Holocene sea-level changes along the Mediterranean coast of Israel, based on archaeological observations and numerical model. Palaeogeography, Palaeoclimatlogy, Palaeoecology 167, 101–117.

Sivan, D., Eliyahu, D., Raban, A., 2004a. Late Pleistocene to Holocene wetlands now covered by sand, along the Carmel Coast of Israel, and their relation to human settlement: an example from the coastal site of Dor. Journal of Coastal Research 20, 97–110.

Sivan, D., Lambeck, K., Toueg, R., Raban, A., Porat, Y., Shirman, B., 2004b. Ancient coastal wells of Caesarea Maritima, Israel, an indicator for sea-level changes during the last 2000 years. Earth and Planetary Science Letters 222, 315–330.

Sneh, Y., Klein, M., 1984. Holocene sea-level changes at the coast of Dor, Southeast Mediterranean. Science 226, 831–832.

Stern, E., 1993. Dor. In: Stern, E., Lewinston-Gilboa, A., Aviram, J. (Eds.), The New Encyclopedia of Archaeological Excavations in the Holy Land, vol. 1. The Israel Exploration Society and Carta, Jerusalem, pp. 357–368.

Stuiver, M., Reimer, P.J., Bard, E., Beck, J.W., Burr, G.S., Hughen, K.A., Kromer, B., McCormac, G., Van der Plicht, J., Spurk, M., 1998a. INTCAL98 radiocarbon age calibration, 24000-0 cal BP. Radiocarbon 40 (3), 1041–1083.

Stuiver, M., Reimer, P.J., Braziunas, T.F., 1998b. High-precision radiocarbon age calibration for terrestrial and marine samples. Radiocarbon 40 (3), 1127–1151.

Vaks, A., Bar-Matthews, M., Ayalon, A., Schilman, B., Gilmour, M., Hawkesworth, C.J., Frumkin, A., Kaufman, A., Matthews, A., 2003. Paleoclimate reconstruction based on timing speleothems growth and oxygen and carbon isotope composition in a cave located in the rainshadow in Israel. Quaternary Research 59, 182–193.

Wieder, M., Yaalon, D.H., 1983. Micromorphology of Hamra soils. In: Grossman, D. (Ed.), Between Yarkon and Ayalon. Bar-Ilan University, Ramat-Gan, pp. 27–34 (in Hebrew).

Yaalon, D., 1959. Classification and nomenclature of soils in Israel. Bulletin of Research Council of Israel 8 (2–3), 91–118.

Yaalon, D.H., Dan, J., 1967. Factors controlling soil formation and distribution in the Mediterranean coastal plain of Israel during the Quaternary. Quaternary Soils, Seventh NQUA Congress, 1965, pp. 321–338.

Yechieli, Y., Magaritz, M., Levy, Y., Weber, U., Kafri, U., Woelfli, W., Bonani, G., 1993. Late Quaternary geological history of the Dead Sea area, Israel. Quaternary Research 39, 59–67.

Yechieli, Y., Gavrieli, I., Berkoeitz, B., Ronen, D., 1998. Will the Dead Sea die? Geology 26 (8), 755–758.